FIGURE 24

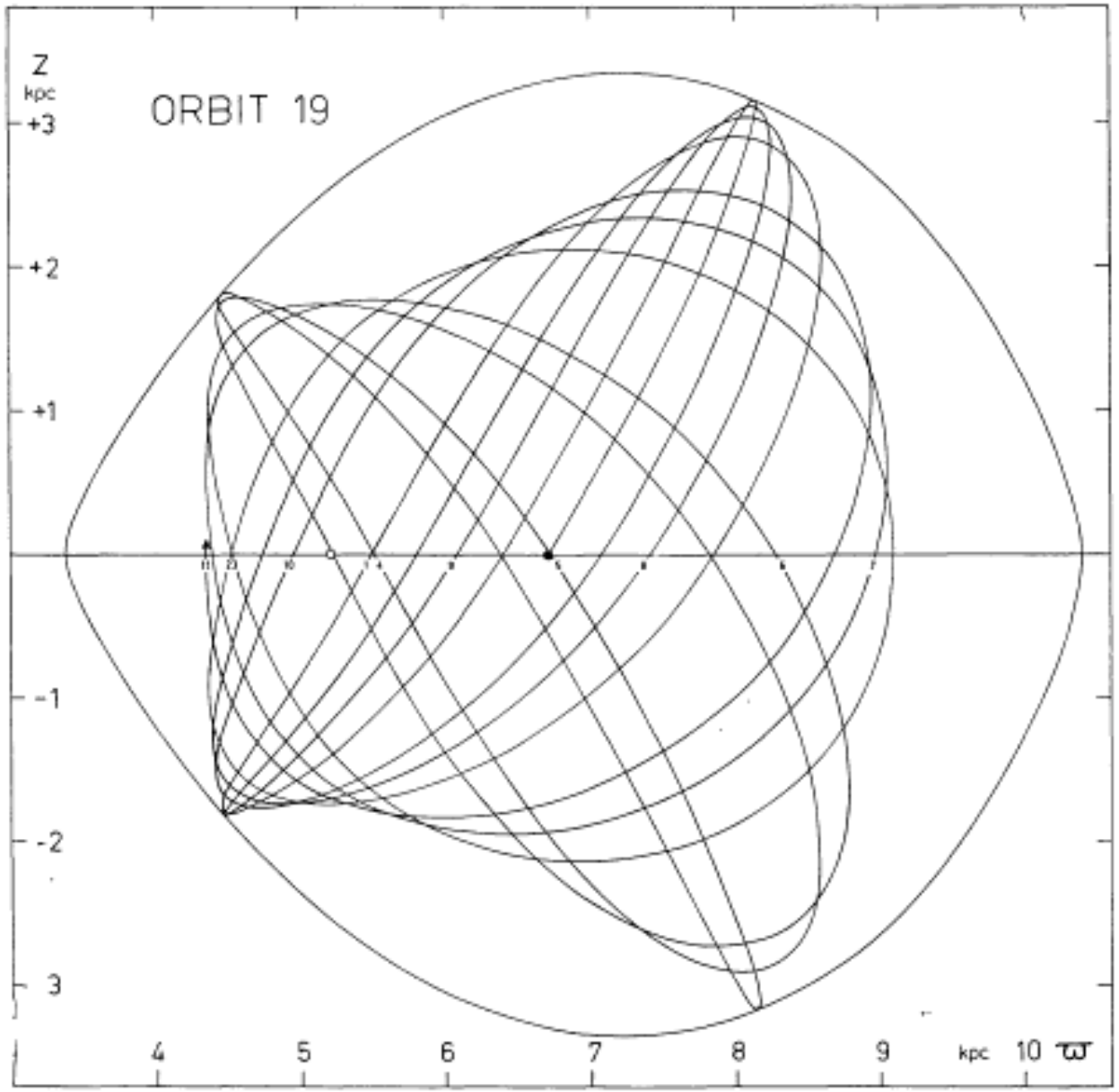

Orbit 19, *intermediate*. In revolution 11 the fundamental point A is approached closely. Motion of orbital plane is shown in Figure 33.

Ollongren (1962)

"Quite unexpectedly, all these orbits behaved as if they had not 2, but 3 isolating integrals. As a result there was some change of opinion on the subject

(Henon & Heiles 1964)

these four initial values, the trajectory can be integrated to the next point satisfying (9), which is P_{i+1}.] It can also be shown that the mapping is area-preserving [see, e.g., Birkhoff (1927, p. 152); and see Moser (1962) for an important theorem concerning such mappings].

3. RESULTS

After some trials, the following potential was chosen for study:

$$U(x,y)=\tfrac{1}{2}(x^2+y^2+2x^2y-\tfrac{2}{3}y^3) \qquad (11)$$

because: (1) it is analytically simple; this makes the computation of the trajectory easy; (2) at the same time, it is sufficiently complicated to give trajectories which are far from trivial, as will be seen below. It seems probable that the potential (11) is a typical representative of the general case, and that nothing would be fundamentally changed by the addition of higher-order terms.

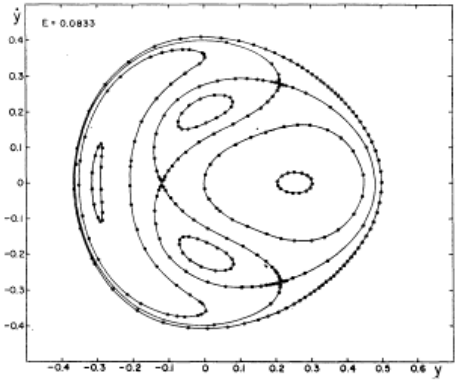

FIG. 4. Results for $E=0.08333$.

Figure 2 shows the equipotential lines. Near the center they tend to be circles; farther out they become elongated in three directions. The particular equipotential $U=\frac{1}{6}$ consists of three straight lines, forming an equilateral triangle.

A number of orbits were computed by numerical integration of the equations of motion:

$$\dot{x}=-\partial U/\partial x=-x-2xy,$$
$$\dot{y}=-\partial U/\partial y=-y-x^2+y^2. \qquad (12)$$

As a check, some of the orbits were computed independently by each of us, using different computers (CDC 1604 and IBM 7090) and different integration schemes (Adams and Runge–Kutta). The following results were obtained using the Runge–Kutta method; during the numerical integration the energy was observed to decrease very slightly ($<|0.00003|$ for 150 orbits).

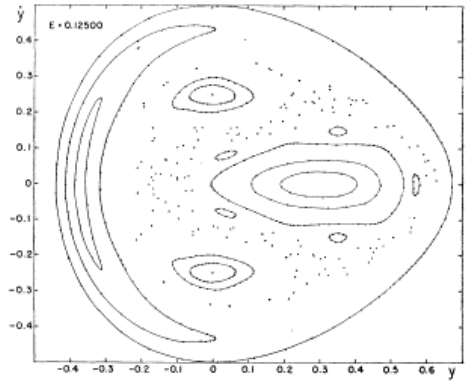

FIG. 5. Results for $E=0.12500$.

Figure 3 shows a set of points P_i for a typical trajectory. They seem to lie exactly on a curve. In fact, more points have been computed than those plotted here; after the 150th point there is still no perceptible deviation from a curve. It may be interesting to remark that the successive points P_1, P_2, $P_3\cdots$ (represented here by 1, 2, $3\cdots$) rotate regularly around the curve. The figure is topologically identical to one where the points P_i would lie on a circle of center O, the angle between OP_i and OP_{i+1} having a constant value α. This constant is not the same for different trajectories. In the case of Fig. 3, its approximate value is $\alpha=0.1143$ (taking one revolution as the unit). α is generally not rational, so that no point P_i will come back exactly on the initial point P_1, and the infinite set of the points P_i is dense everywhere on the curve. If α happens to be a rational number p/q, the point P_{q+1} will be identical with P_1 and the orbit is periodic.

Figure 4 shows the complete picture in the $(y,\dot{y})$ plane, for a given value of the energy: $E=\frac{1}{12}=0.08333$.

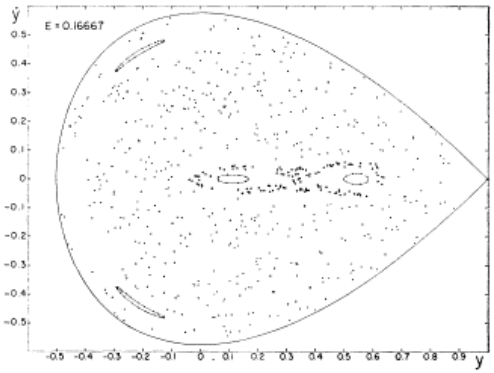

FIG. 6. Results for $E=0.16667$.

Henon & Heiles (1964)

box orbit

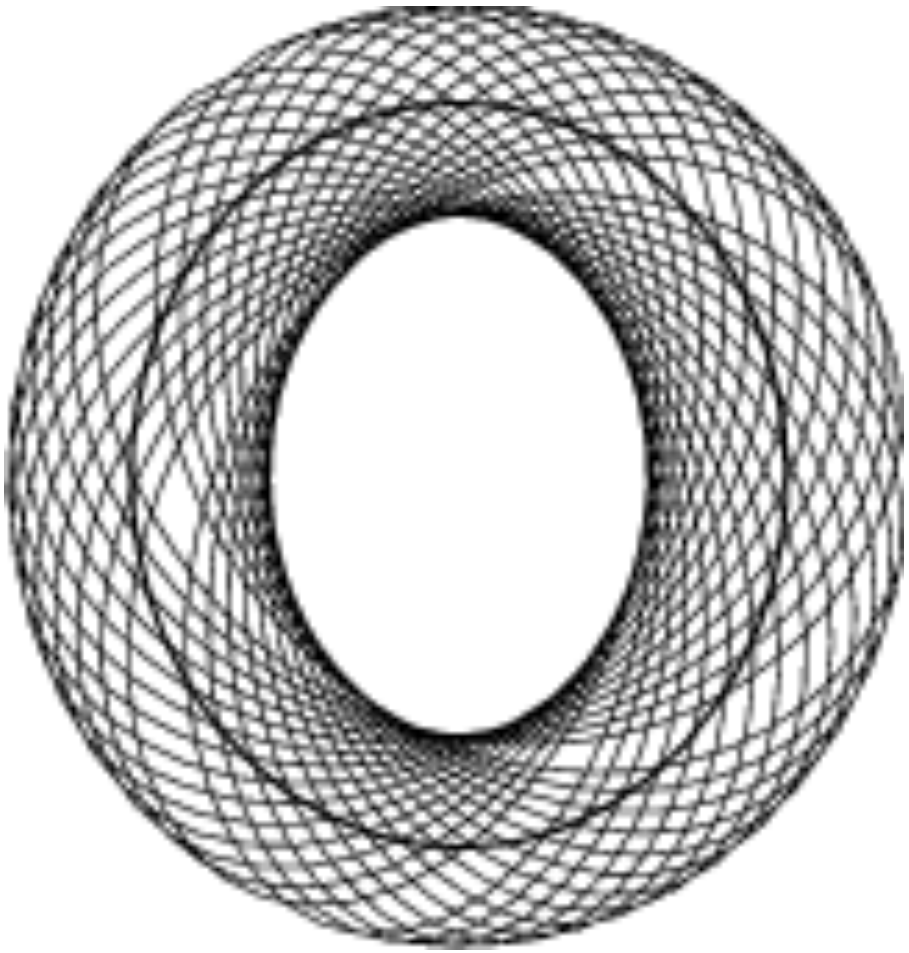

loop orbit

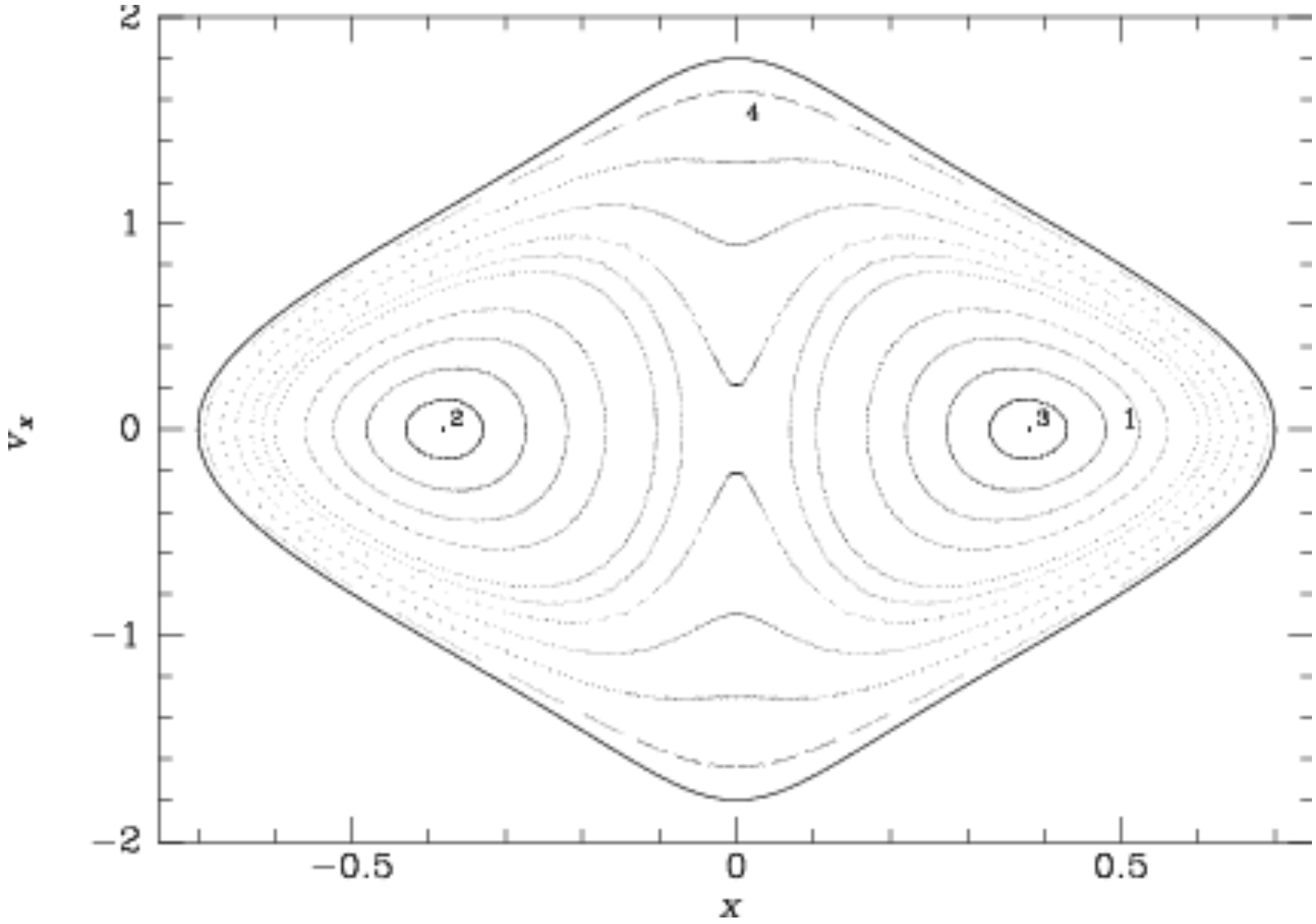
2
1
0
−1
−2
v_x
−0.5
0
0.5
x
4
2
3
1

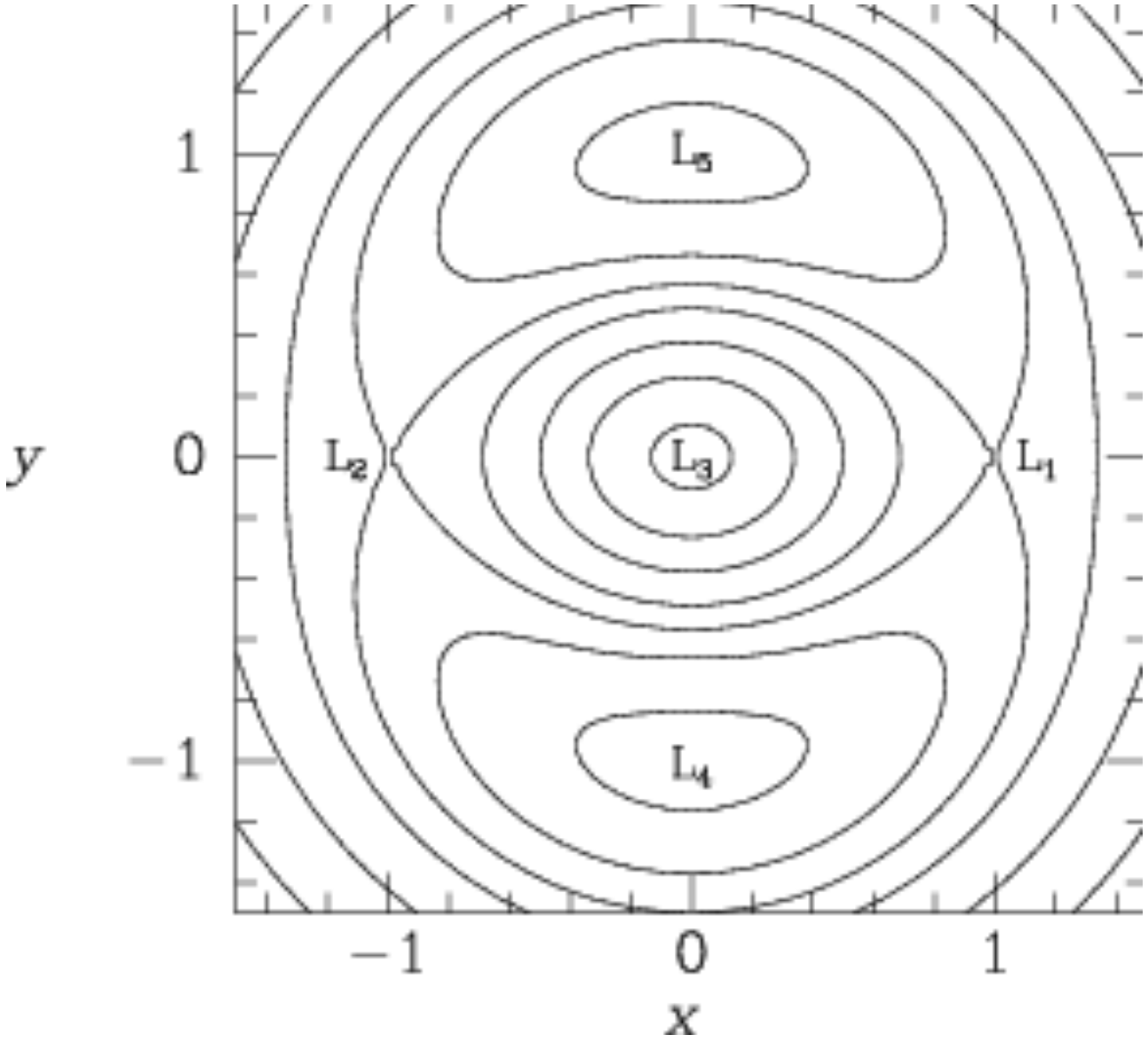
L5
L2
L3
L1
L4
1
0
−1
y
−1
0
1
x

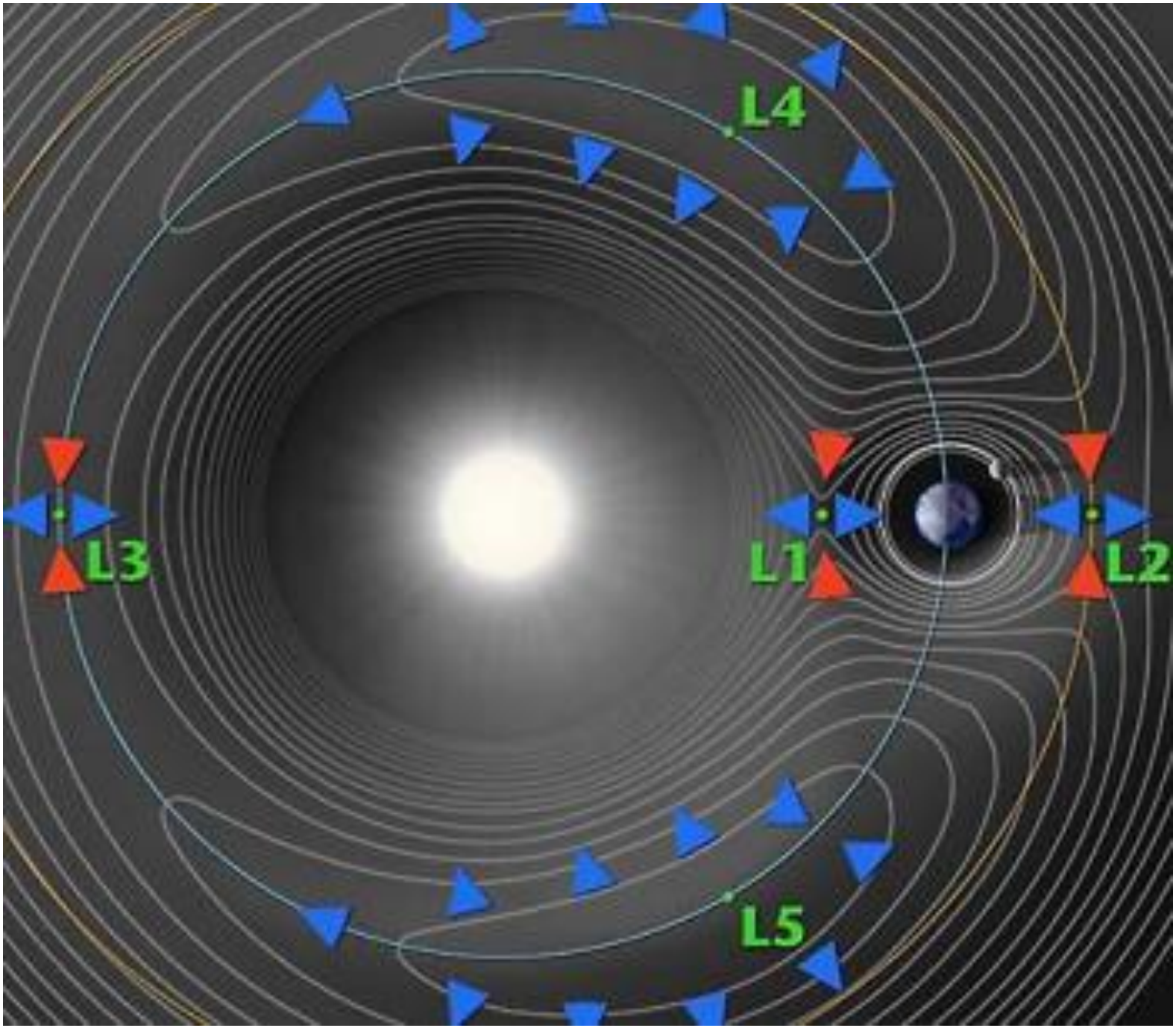
L4
L3
L1
L2
L5

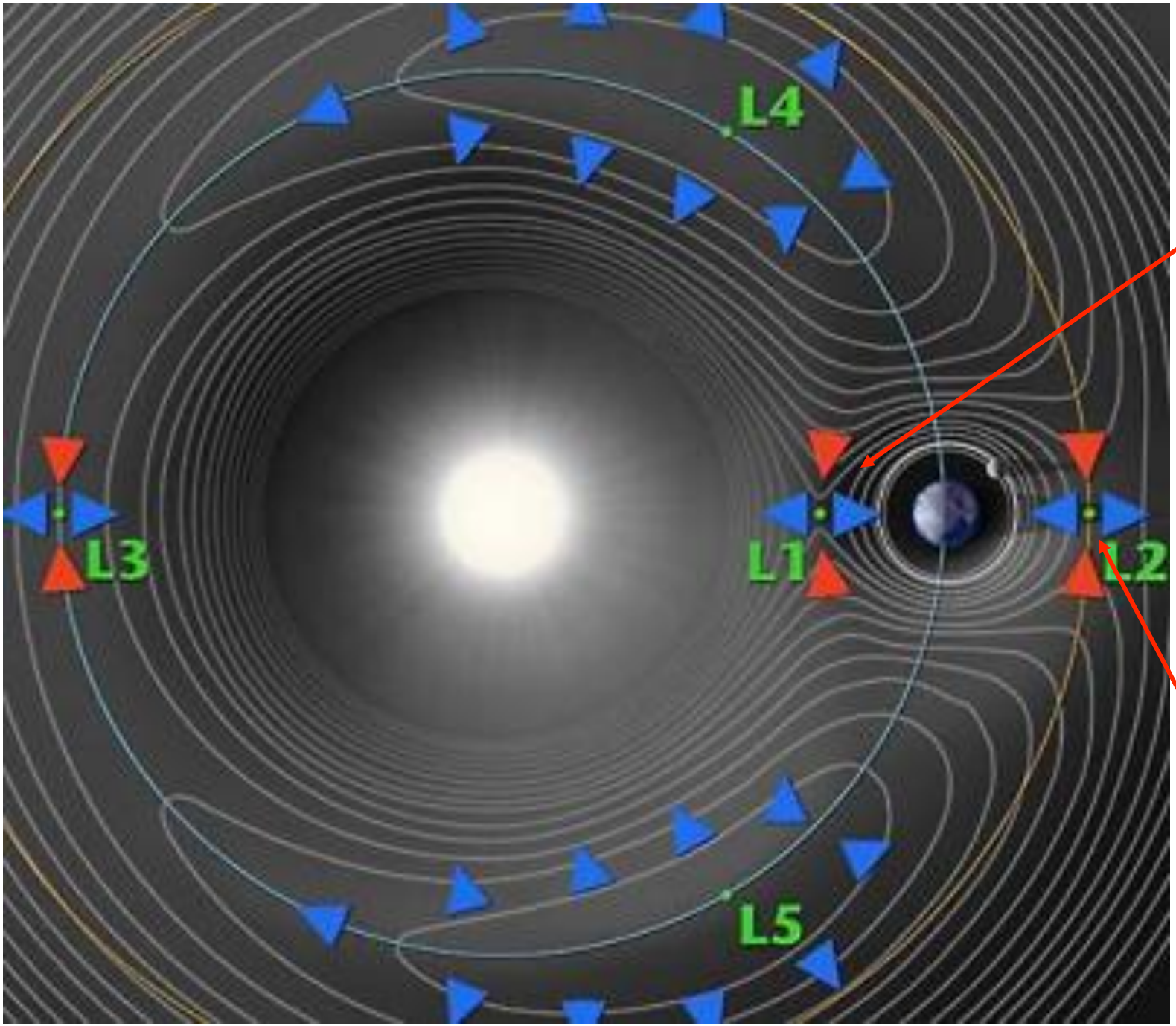
L4
L3
L1
L2
L5
SOHO
WMAP
Planck
JWST

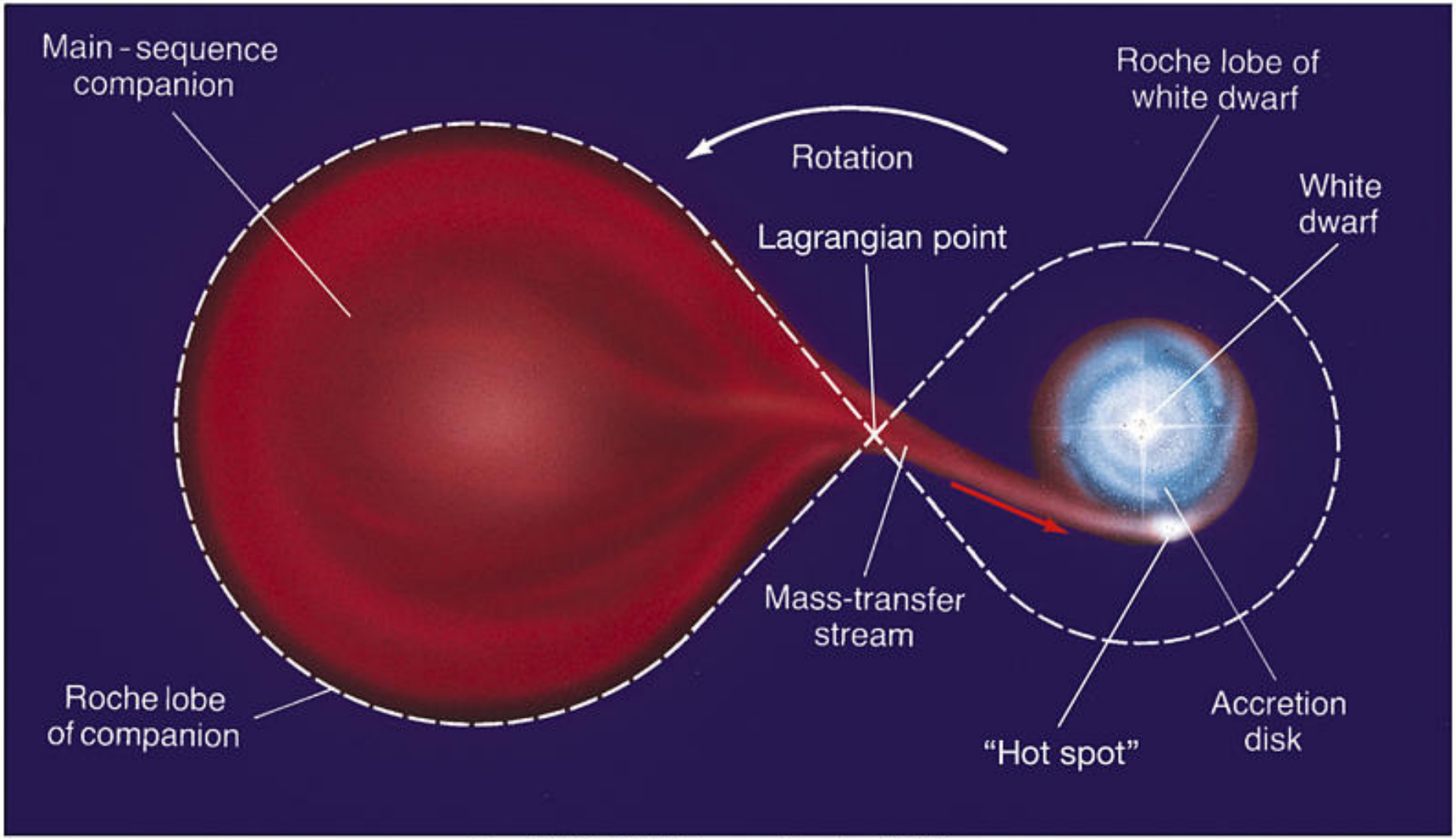

Trojan asteroids

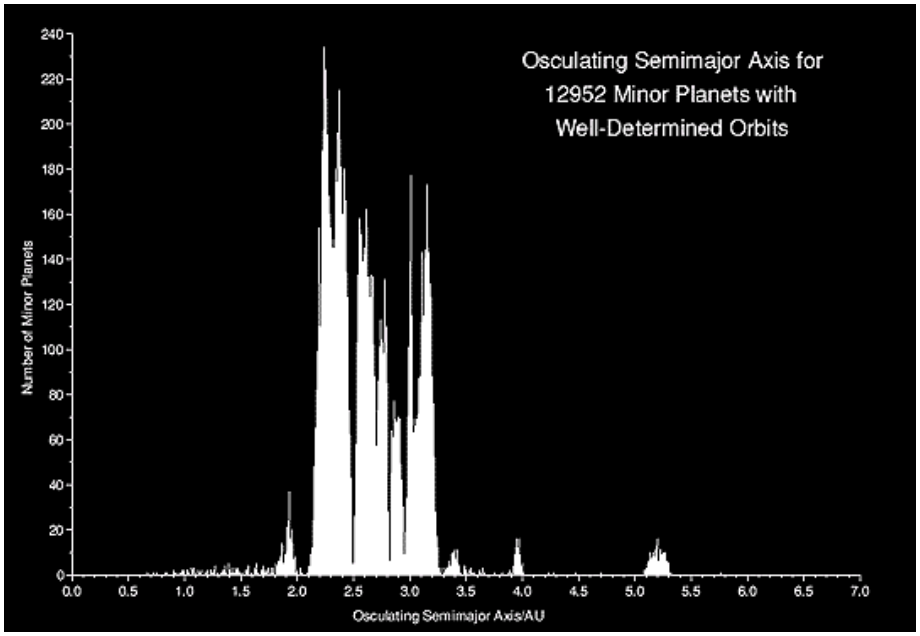

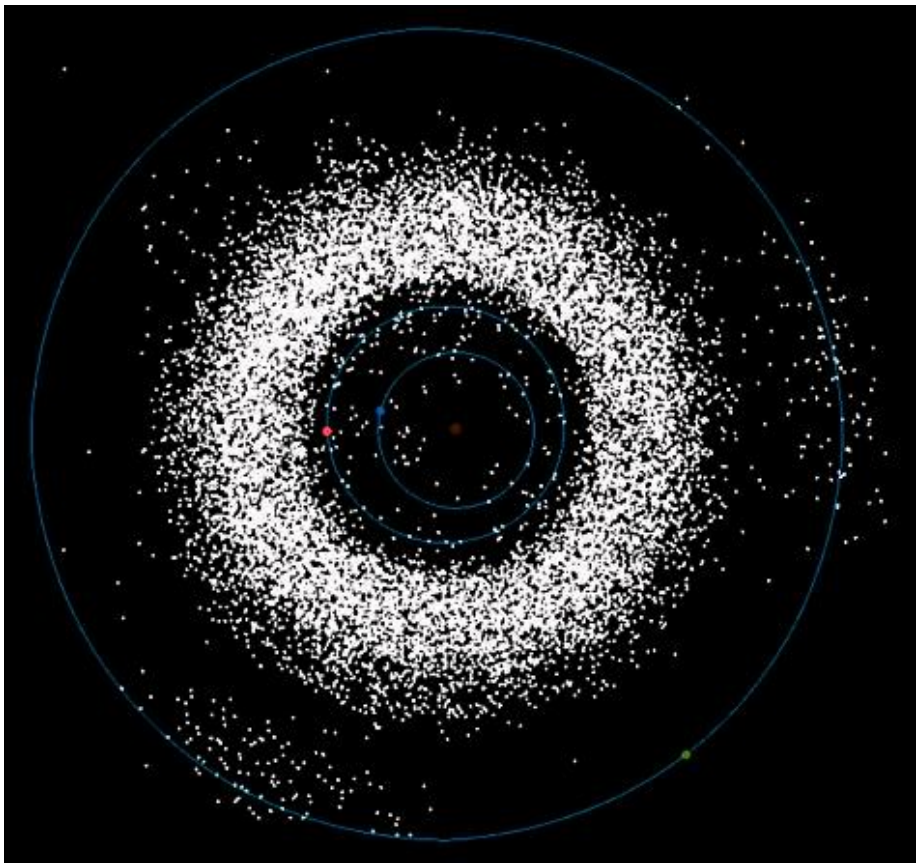

a(Jupiter)=5.2 AU

models of omega Centauri using Schwarzschild's method (van de Ven 2005)

G. van de Ven et al.: The dynamical distance and intrin

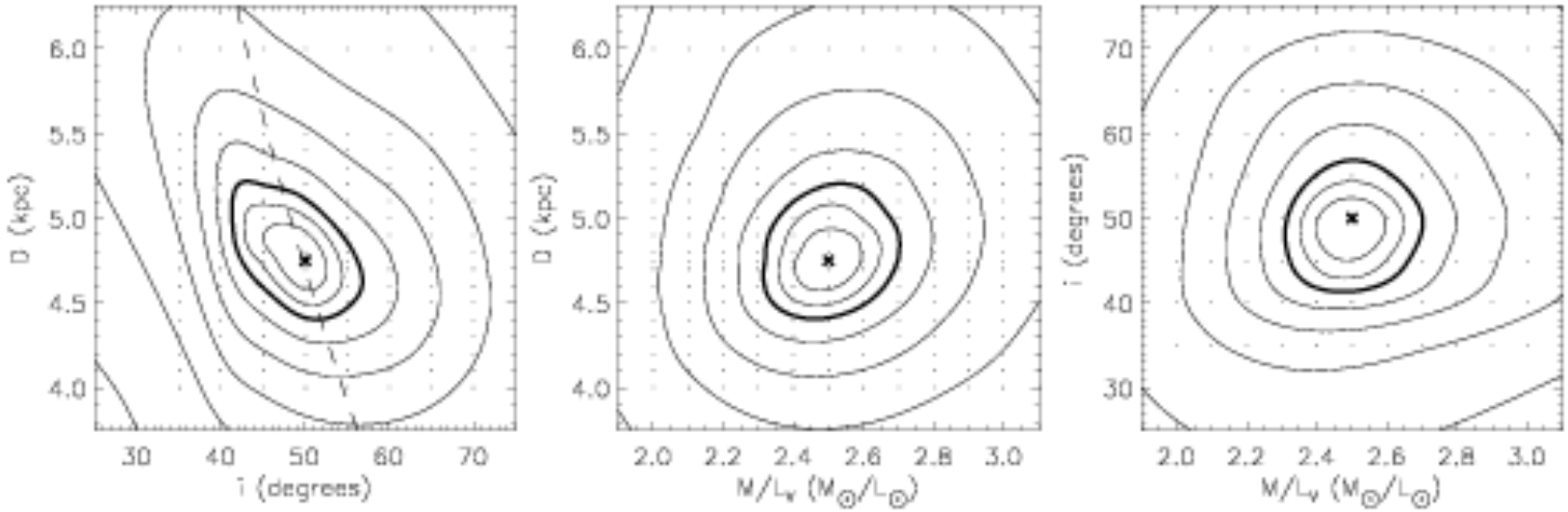

Fig. 15. The (marginalised) goodness-of-fit parameter $\Delta\chi^2$ as a function of distance D, inclination i and mass-to-light ratio M/L_V, for different dynamical model fits (indicated by the dots) to the kinematics of ω Cen. The contours are as in Figure 10. The best-fit dynamical model is at $D = 4.8$ kpc, $i = 50°$ and $M/L_V = 2.5$ $M_\odot/L_\odot$, indicated by the cross The dashed curve shows the $D \tan i = 5.6$ kpc constraint from the mean velocities (§ 4.5).

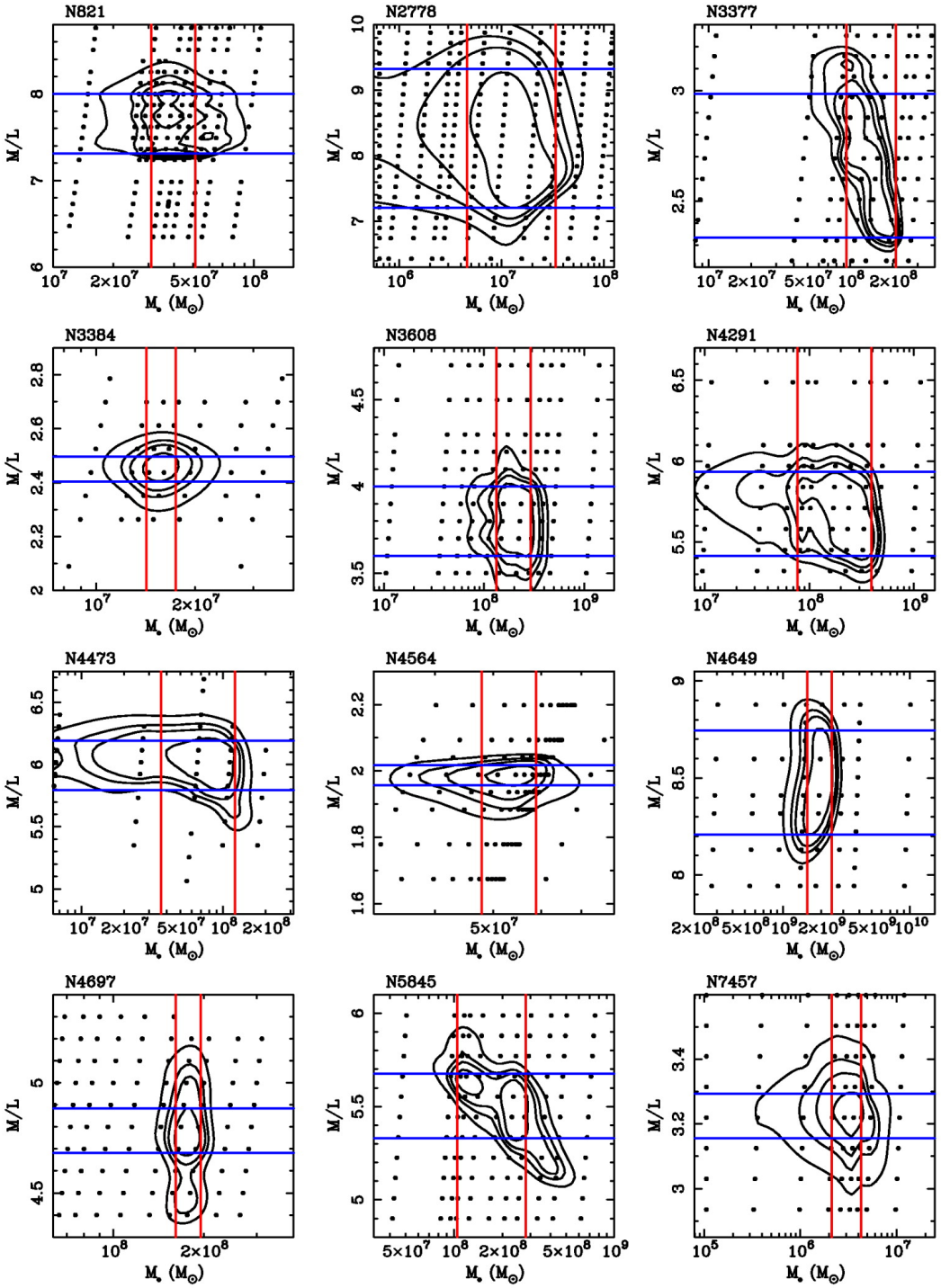

evidence for black holes in elliptical galaxies using Schwarzschild's method Gebhardt et al. (2003)

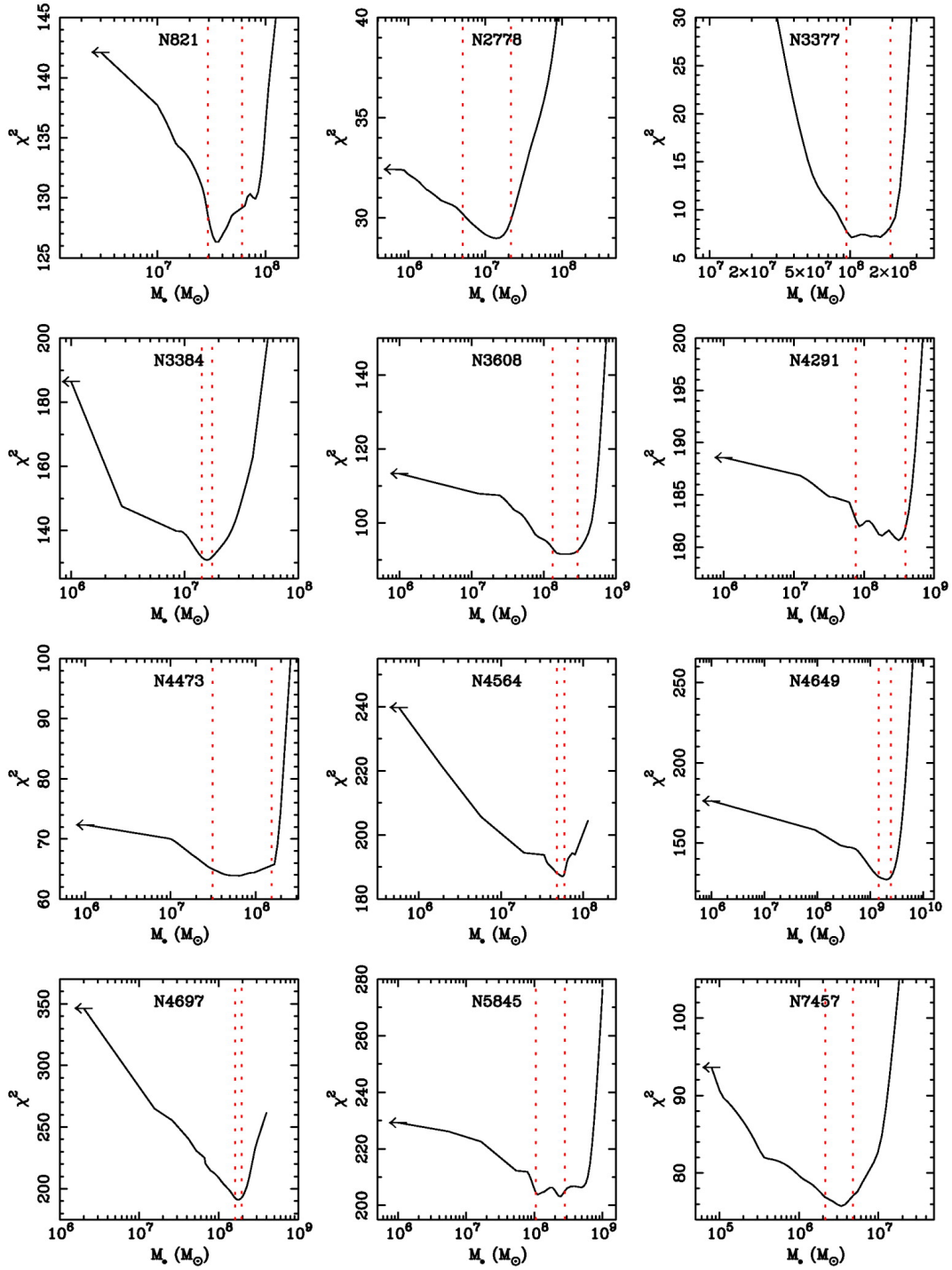

evidence for black holes in elliptical galaxies using Schwarzschild's method Gebhardt et al. (2003)

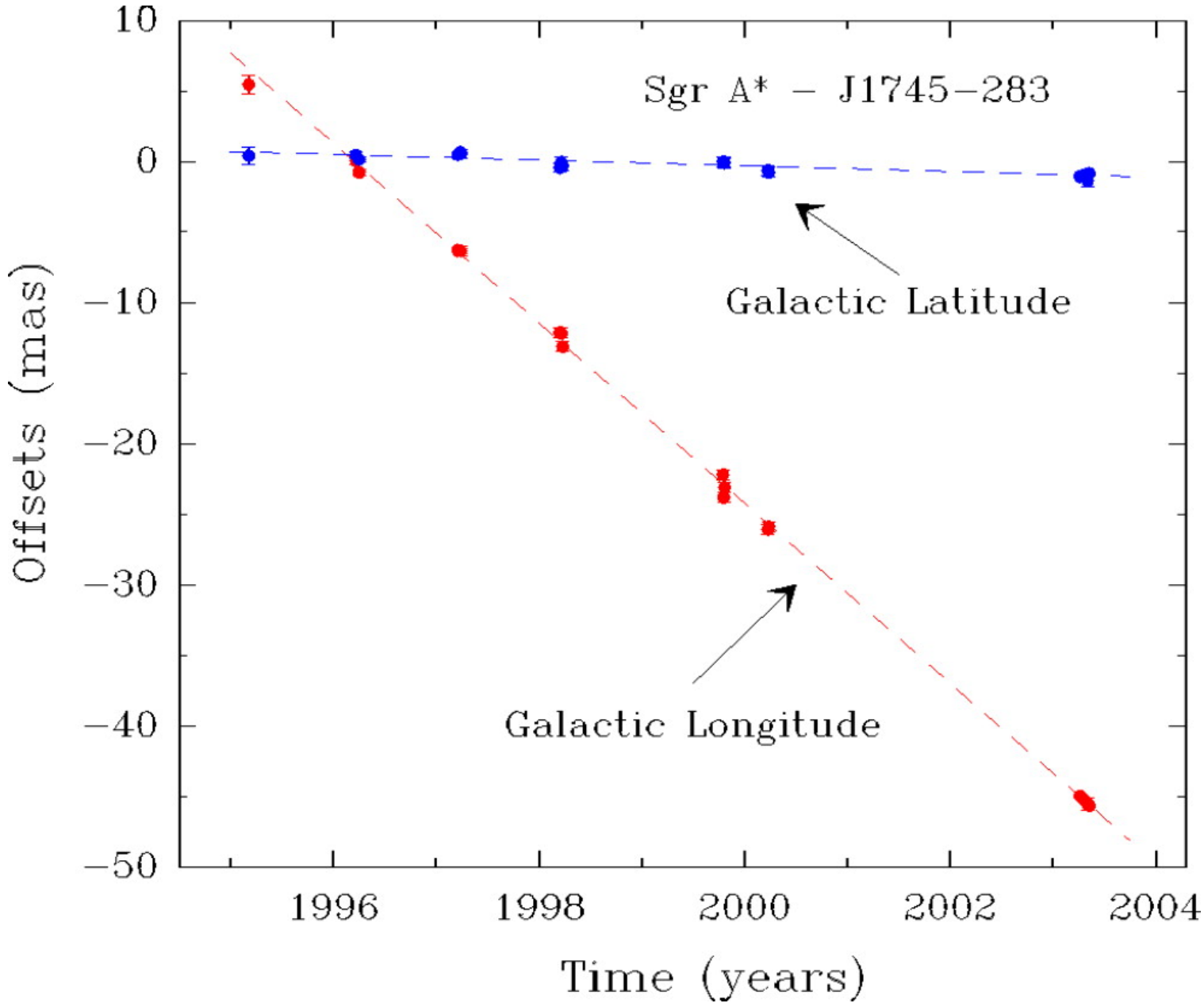

Proper motion (angular speed) of Sgr A* (Reid et al. 2005)

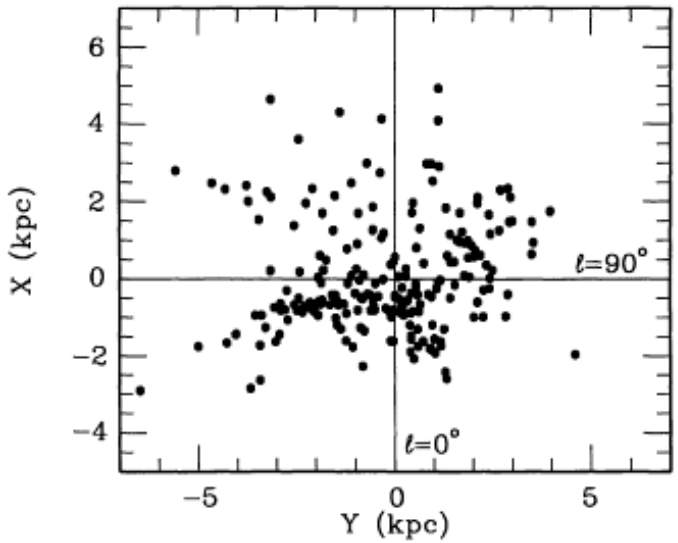

Figure 1. The distribution of the Cepheids used in the proper motion solutions seen projected on to the Galactic Plane. The Sun is at the origin of the coordinate system. The distances are from the PL relation derived in Paper I.

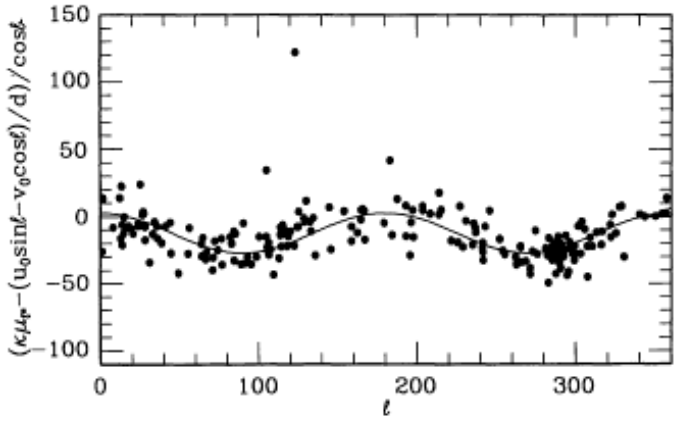

Figure 2. The proper motion in Galactic longitude multiplied by κ, and corrected for local solar motion, plotted against Galactic longitude. The curve corresponds to solution 2 of Table 4. The three outstanding stars are nearby and have low weight in the solution (see text for further details).

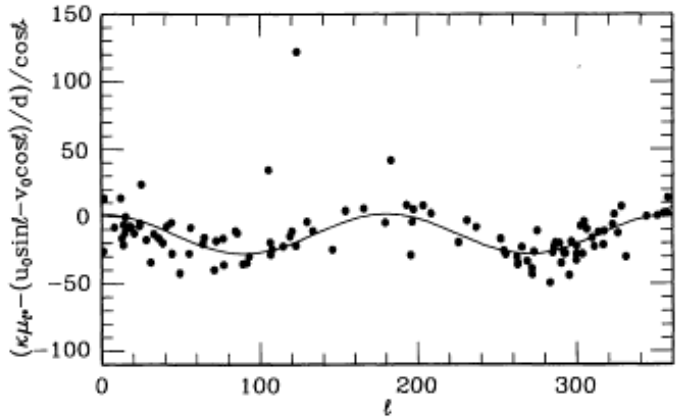

Figure 3. As Fig. 2 but for stars with distances less than 2 kpc. The curve illustrates solution 5 of Table 4.

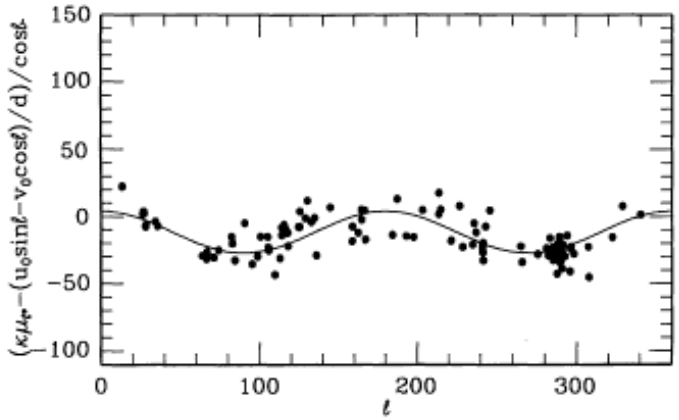

Figure 4. As Fig. 2 but for stars with distances equal to or greater than 2 kpc. The curve illustrates solution 6 of Table 4.

The quantity $[\kappa\mu_{\ell*} - (u_\circ \sin\ell - v_\circ \cos\ell)/d]/\cos b$ is shown in Fig. 2, plotted against Galactic longitude (ℓ) for solution 2 of Table 4. Figs 3 and 4 show similar plots for the nearer and more distant stars (solutions 5 and 6), the curves in each case illustrate the corresponding solutions in Table 4.

Whilst the effect of Galactic rotation on proper motions has long been known (e.g. Oort 1927), it does not seem to

Feast & Whitelock (1997)

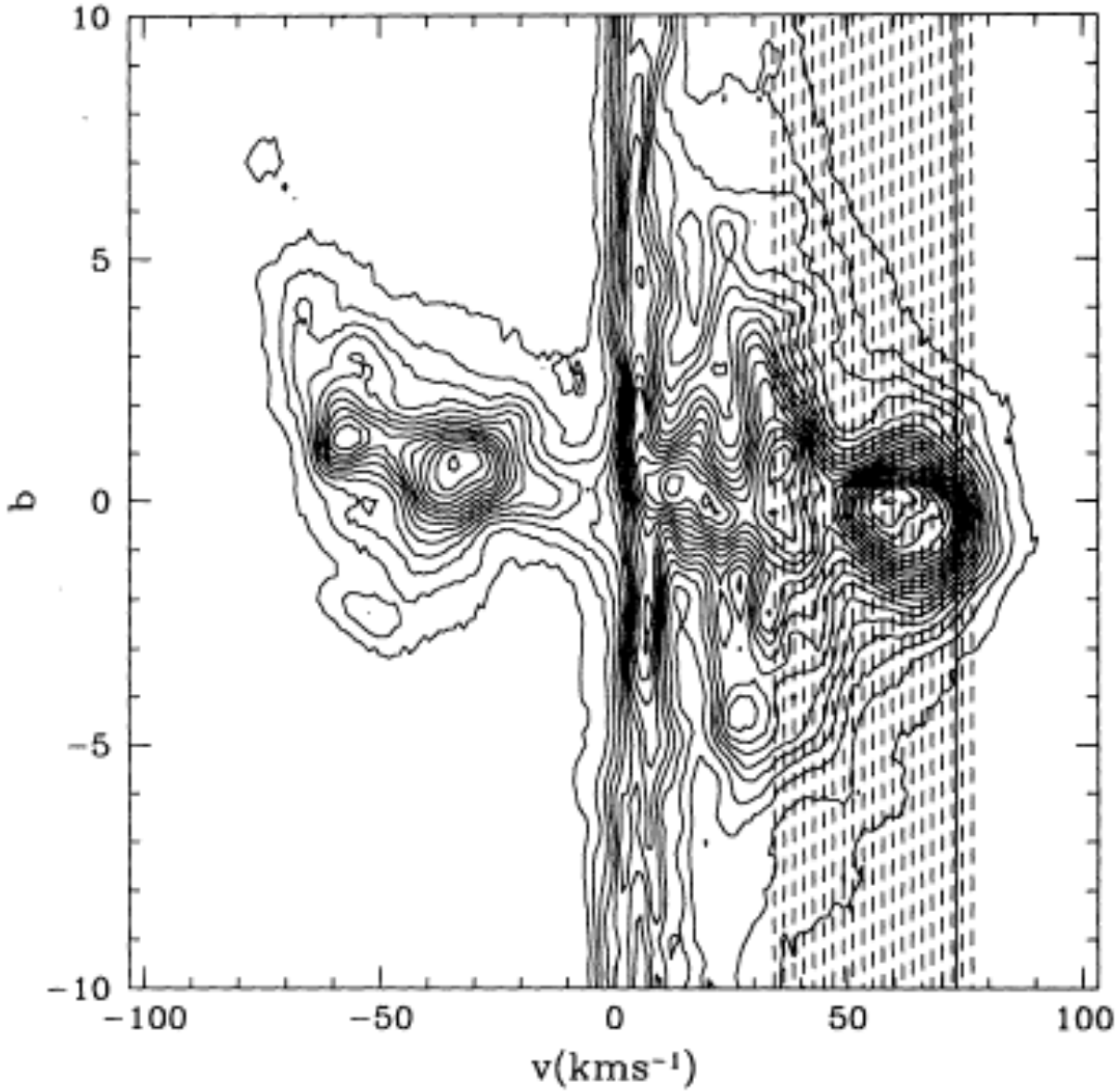

Malhotra (1995)

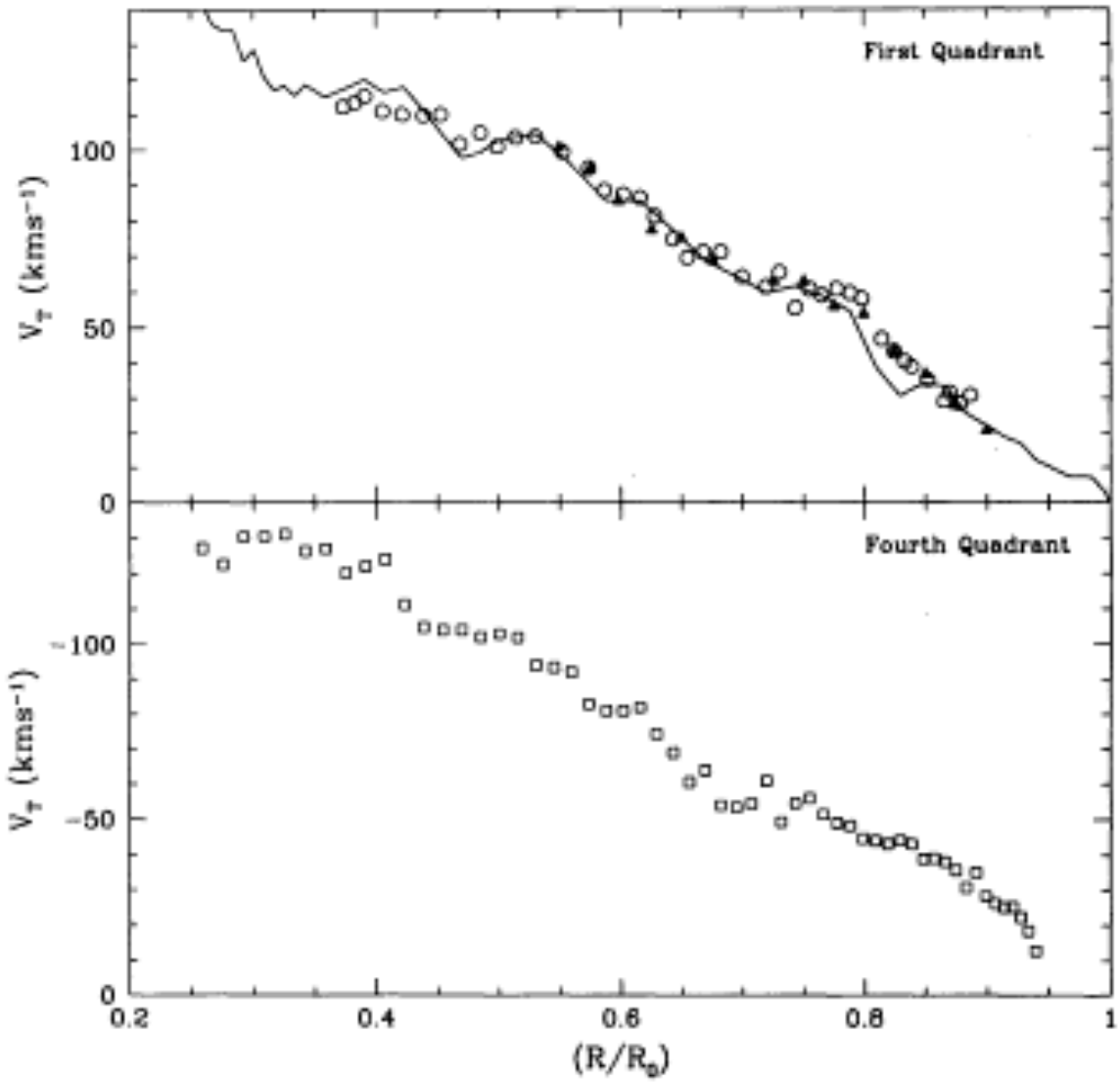

FIG. 7.—The terminal velocity V_T for the tangent point gas at different Galactic longitudes l (hence Galactic radii $R/R_0 = \sin(l)$]. The solid line shows the terminal velocity for H I from Gunn et al. 1979 (*open circles*: WW survey; *triangles*: BL survey; *open squares*: Parkes survey).

Malhotra (1995)

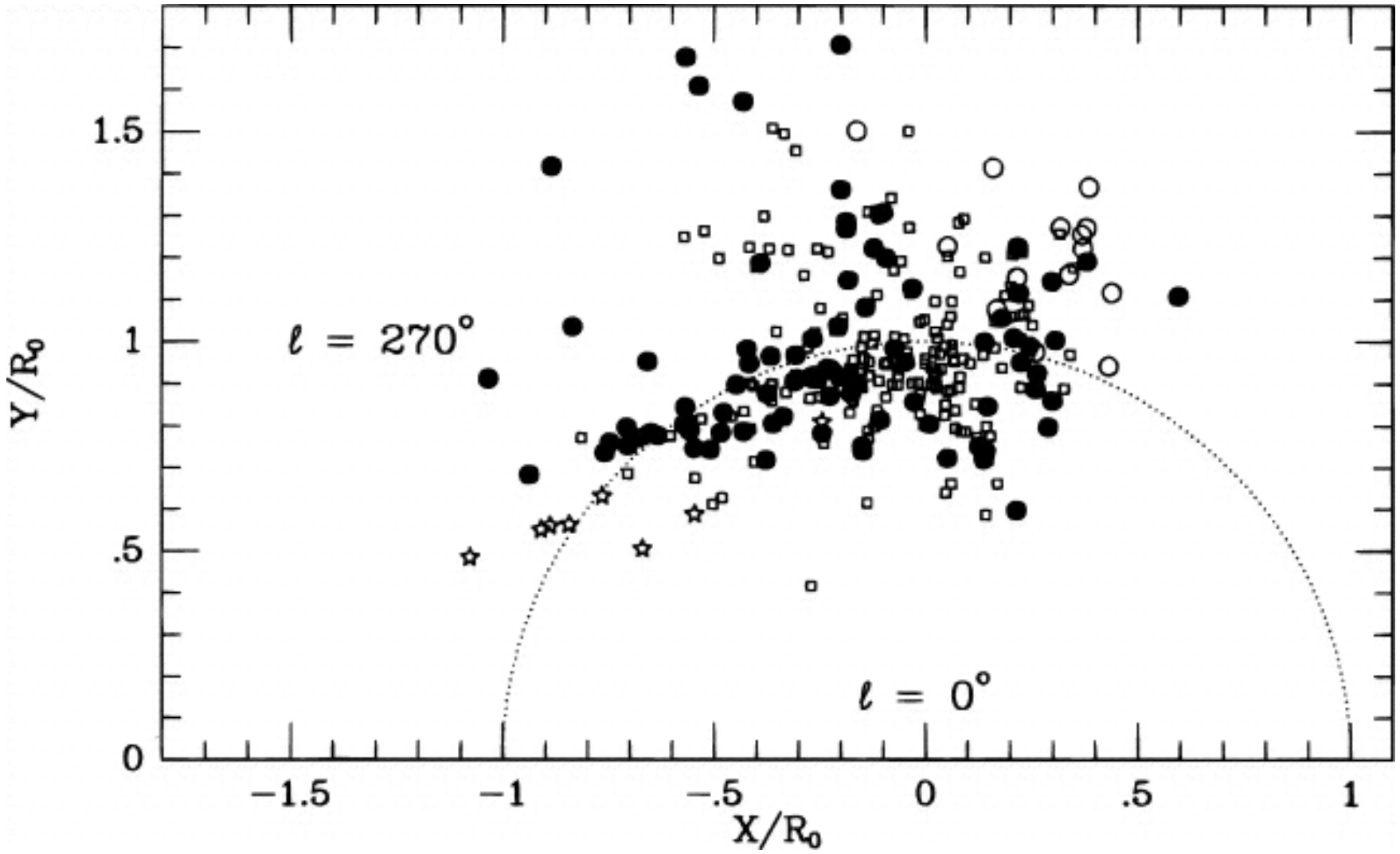

Metzger et al. (1998)

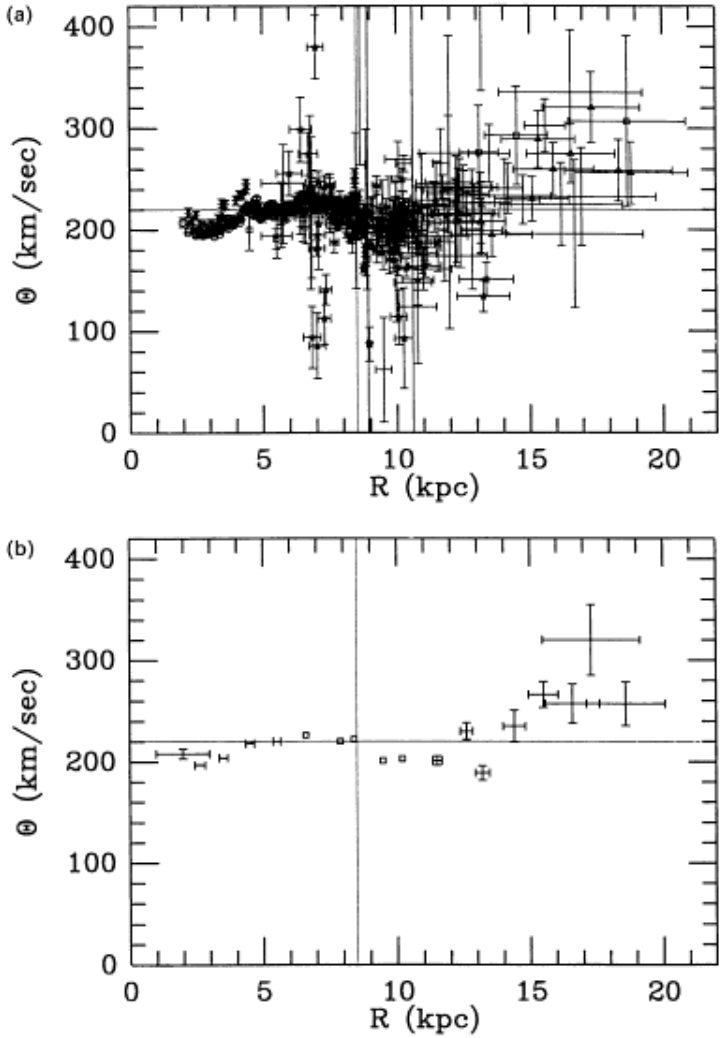

Figure 2 The rotation curve of the Galaxy for the 1985 IAU values $R_o = 8.5$ kpc, $\Theta_o = 220$ km s^{-1} (*dotted lines*). (*a*) Individual data points and associated error bars. Open squares: planetary nebulae from Schneider & Terzian (1983); open circles: CO tangent points from Clemens (1985); open triangles: H II regions from Chini & Wink (1985); stars: open clusters from Hron (1987); asterisks: H I tangent points from Burton & Gordon (1978); naked error bars: H II regions from Fich et al (1989). (*b*) Averaged rotation curve using data in (*a*). The error bars are plotted using the overly optimistic assumption that errors in R and Θ, as well as errors in different data points, are all Gaussian and uncorrelated. Open squares denote cases in which the error bar is smaller than the size of the symbol. Errors in distances determined by the tangent point method are taken to be 1 kpc.

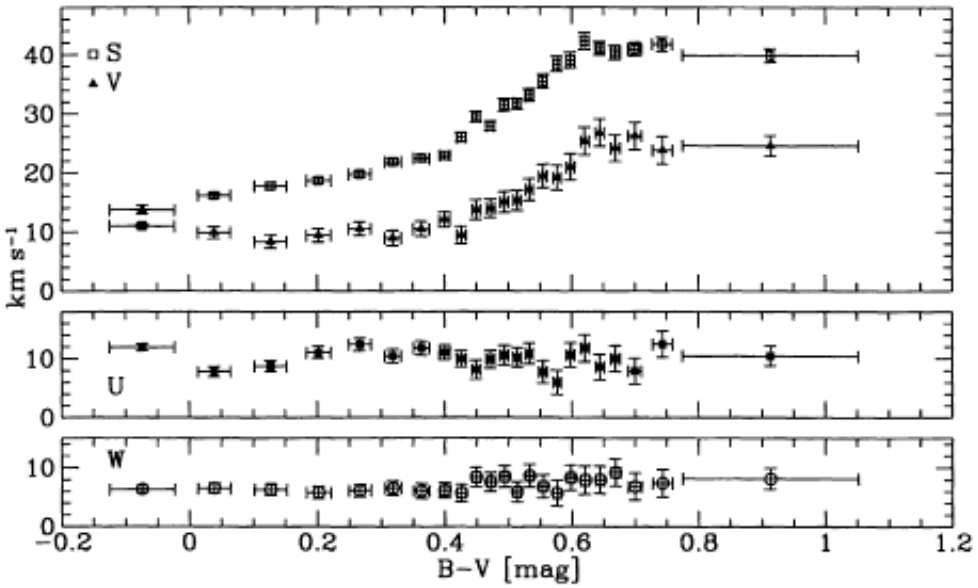

Dehnen & Binney (1998)

Figure 3. The components U, V and W of the solar motion with respect to stars with different colour $B - V$. Also shown is the variation of the dispersion S with colour.

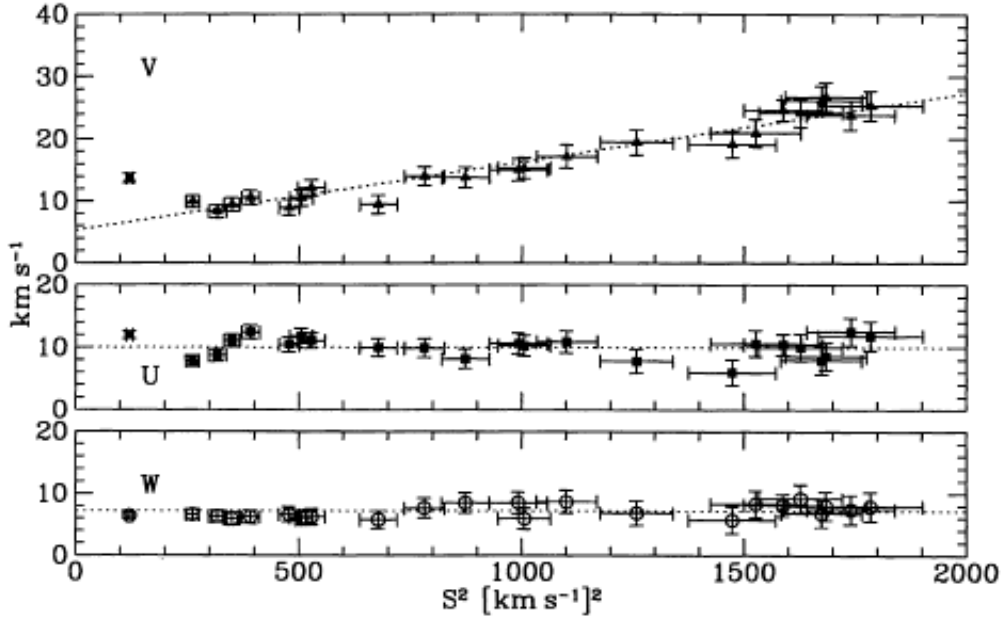

Figure 4. The dependence of U, V and W on S^2. The dotted lines correspond to the linear relation fitted (V) or the mean values (U and W) for stars bluer than $B - V = 0$.

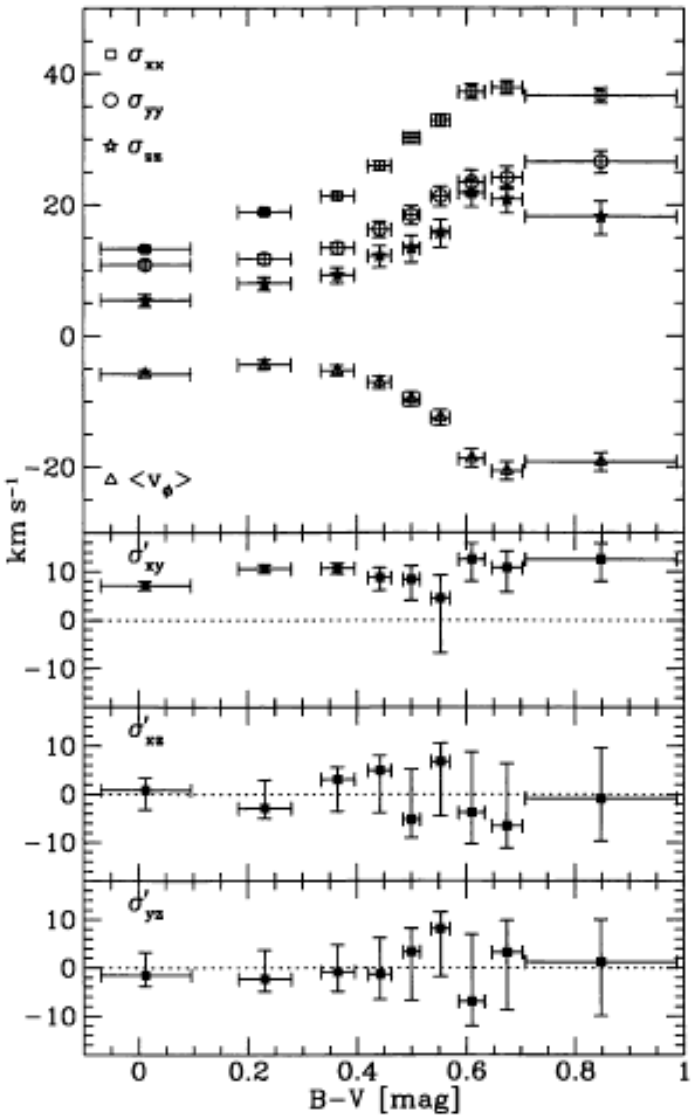

Figure 5. Velocity dispersions for stars in different colour bins. The top panel shows the mean rotation velocity (negative values imply lagging with respect to the LSR) and the three main velocity dispersions. In the three bottom panels $\sigma'_{ij} = \mathrm{sign}(\sigma^2_{ij})\,|\sigma^2_{ij}|^{1/2}$ is plotted for the mixed components of the tensor σ^2_{ij}.

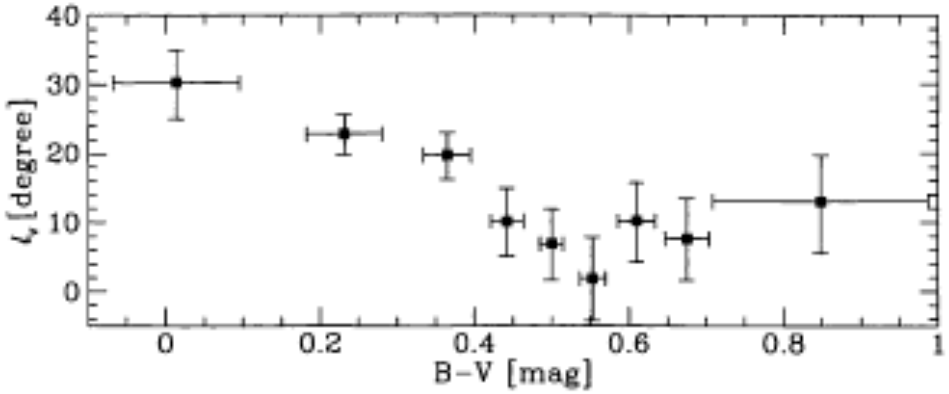

Figure 6. The vertex deviation ℓ_v versus $B-V$ colour. The error bars correspond to the 15.7 and 84.3 percentiles (i.e. 1σ error) and have been obtained assuming a multivariate Gaussian distribution in the σ^2_{ij} with variance evaluated via equation (15).

Dehnen & Binney (1998)

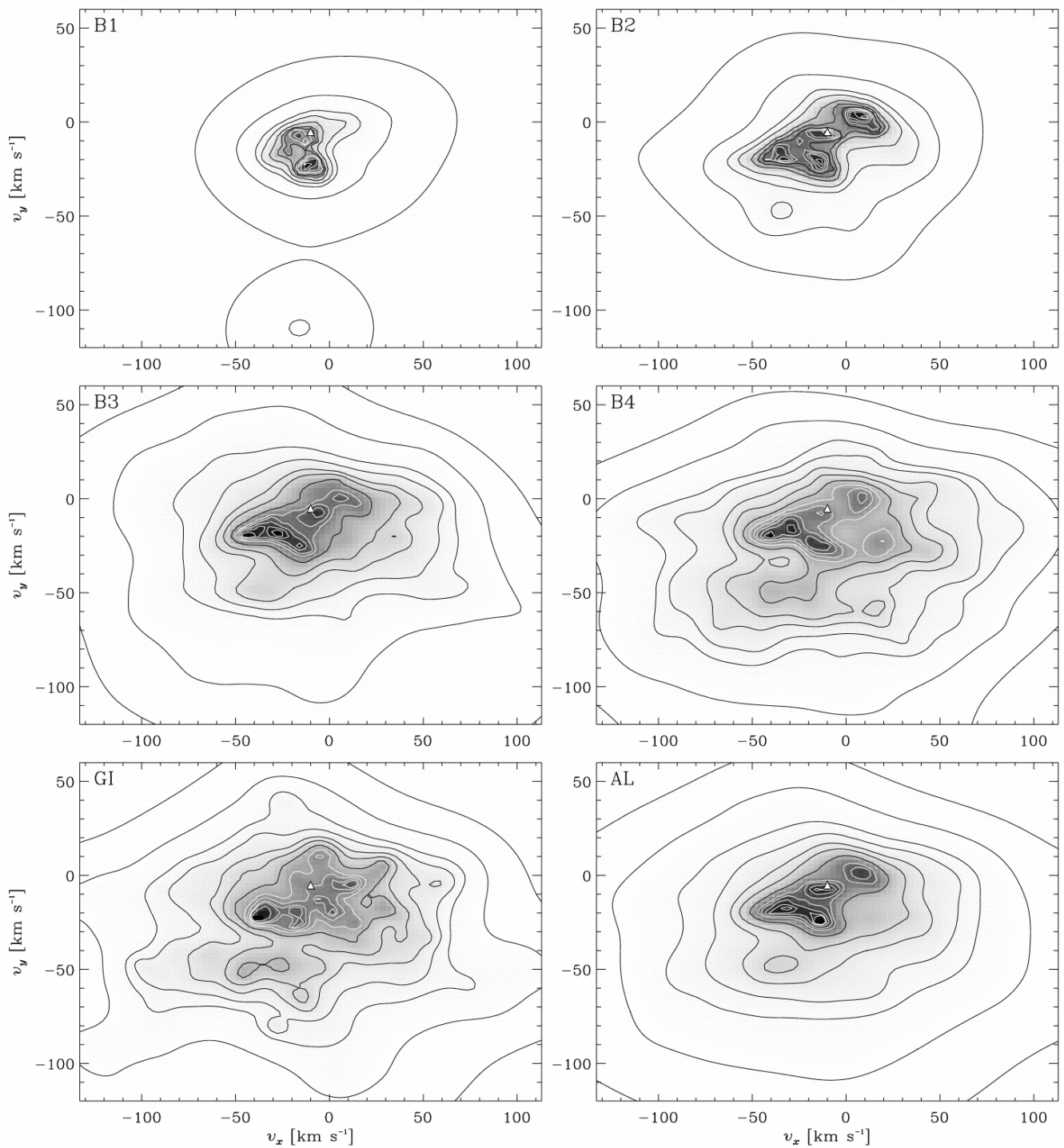

Dehnen (1998)